Supporting Information for

Methyl group in asymmetric DPP n-type copolymers impedes aggregation and charge transport anisotropy

Thomas Müller,[1] *Pierluigi Mondelli,*[2] *Tommaso Losi,*[2] *Hartmut Komber,*[3] *Florian Lombeck,*[4†] *Daniele Fazzi,*[5] *Christopher R. McNeill,*[6] *Mario Caironi,*[2] *and Michael Sommer*[1]*

Table of contents

A) General Materials and Methods 2
B) Additional Figures and Tables 5
C) ^{1}H and ^{13}C NMR Spectra 16
D) Supporting References 24

A) General Materials and Methods

Chemicals. All chemicals, reagents and solvents were purchased from commercial sources and used as received unless otherwise noted. Solvents used for column chromatography were distilled under reduced pressure before use. Toluene, tetrahydrofurane (THF), *tert*-amyl alcohol and dimethylformamide (DMF) were dried over molecular sieve (4 Å).

NMR Spectroscopy. NMR spectra were recorded on a Bruker ARX 300 (^{1}H: 300 MHz, ^{13}C: 75 MHz) or Bruker Avance III 500 spectrometer (^{1}H: 500 MHz, ^{13}C: 125 MHz, ^{19}F: 470 MHz). The spectra were referenced to the solvent peak ($CDCl_3$: $\delta(^{1}H) = 7.26$ ppm, $\delta(^{13}C) = 77.16$ ppm; $C_2D_2Cl_4$: $\delta(^{1}H) = 5.98$ ppm, $\delta(^{13}C) = 73.7$ ppm; DMSO-d_6: $\delta(^{1}H) = 2.50$ ppm, $\delta(^{13}C) = 39.99$ ppm). Chemical shifts are given in ppm.

Mass spectrometry. Mass spectra were obtained from a LCQ Advantage / Extractive (Thermo Fisher) instrument in ESI mode.

Elemental analysis. Elemental analysis was performed on a VarioEL (Elementar Analysensysteme GmbH) instrument.

UV-Vis Spectroscopy. UV-Vis absorption spectra in solution were recorded on a Cary 60 UV-Vis (Agilent Technologies). Thin-film absorption spectra were measured on a Flame-S UV-Vis spectrometer from Ocean Optics, controlled by the OceanView 1.5.2 software.

Differential Scanning Calorimetry. DSC measurements were carried out on a DSC 2500 (TA Instruments) in aluminium standard pans under nitrogen atmosphere with a heating-/cooling rate of 10 K/min.

Thermogravimetric Analysis. TGA measurements were performed on a Mettler-Toledo TGA/DSC 3+ with HT/1600/557-DTA sensor in nitrogen atmosphere with a heating rate of 10 K/min.

Size exclusion chromatography. Molecular weights were measured on a Shimadzu system comprising a 5 µm precolumn and three SDplus columns with pore sizes ranging from 10^2 to 10^4 Å (Polymer Standards), connected in series with a RID-20A RI detector and a SPD-M20A photodiode array UV-vis detector (Shimadzu) calibrated with polystyrene standards. $CHCl_3$ was used as eluent at 40 °C with a flow rate of 1.0 mL/min. PS was used for calibration.

*Tight-binding xTB and DFT calculations***.** The geometry optimization of each structure was initially performed at the semiempirical level, namely adopting the density functional tight-binding scheme GFNn-xTB (Geometry Frequency Non-covalent interactions-eXtended Tight Binding, specifically GFN2-xTB.[1] (v. 6.4.1). Most stable conformers and the relaxed potential energy profile were computed at the DFT level. For the DFT calculations the B3LYP functional with the inclusion of dispersion corrections (i.e., the atom-pairwise dispersion correction with the Becke-Johnson damping scheme D3BJ scheme) was considered. The basis set adopted was the def2-TZVP (valence triple-zeta polarization) for all atoms. Tight-binding semiempirical calculations were carried out by using the code xTB. DFT calculations were carried out by using the code ORCA v.5.0.3.[2]

OFET preparation and electrical measurement. FETs were fabricated using a top-gate, bottom-contact architecture. Source and drain interdigitated electrodes (channel width, W = 5000 μm; channel length, L_C = 35 μm) were defined by standard lift-off photolithography (3 nm thick Cr adhesion layer and 30 nm thick Au) on glass substrates (low alkali 1737F Corning glasses, purchased from Apex Optical Services). Patterned substrates were washed in an ultrasonic bath of acetone, isopropyl alcohol 5 minutes each before deposition of the semiconductors. P1H and P2Me thin films (30 –50 nm) were casted from toluene (5 g/l) through off-center spin coating (60 s, 1000 rpm) and treated at different temperatures (in the 120 – 350 °C range) for 30 min. A ~550 nm thick PMMA dielectric layer was casted at 1000 rpm for 60 seconds from a 80 g/L tert-butyl alcohol solution. As the gate electrode, a thermally evaporated 40 nm thick Al layer was employed.

The fabricated transistors were measured after an overnight annealing at 110 °C in a nitrogen glovebox on a Wentworth Laboratories probe station with an Agilent B1500A semiconductor device analyzer. The saturation field-effect mobility (μ_{sat}) was extracted from the transfer characteristic curves according to the gradual channel approximation, following the expression:

$$\mu_{sat} = \frac{2L_C}{C_{diel}W}\left(\frac{\partial\sqrt{|I_{DS}|}}{\partial V_{GS}}\right)^2$$

where I_{DS} is the source-drain current, C_{diel} is the dielectric capacitance per unit area, W and L_C are the channel width and channel length, and V_{GS} and V_{DS} are the gate-source and drain-source applied voltages.

Optical microscopy. Polarised optical microscope images were acquired on a Zeiss Axio Scope A1 equipped with a single polariser (Epipol mode) and using a 10X magnification.

GIWAXS. GIWAXS measurements were performed at the SAXS/WAXS beamline at the Australian Synchrotron.[3] 15 keV photons were used with the 2D scattering patterns recorded using an in-vacuum Pilatus 2M detector with the sample-to-detector distance of ~ 67 cm calibrated using a silver behenate reference standard. The sample and detector were enclosed in a vacuum chamber to suppress air scatter. A total exposure time of 3 s was used with the reported 2D images being the composite of three 1s shots taken at different lateral detector positions to fill the gaps between the detector modules. Scattering patterns were measured as a function of angle of incidence, with data shown acquired with an angle of incidence near the critical angle that maximized scattering intensity from the sample. Data reduction and analysis was performed using an altered version of NIKA analysis package implemented in Igor Pro.[4]

B) Additional Figures and Tables

Polymerization conditions

Table S1. Reaction conditions for PThDPPMeThF4. Tris(dibenzylideneacetone)dipalladium(0) (Pd_2dba_3) as catalyst (4 mol-%) and tris(2-methoxyphenyl)phosphine (P(*o*-anisyl)$_3$) as ligand (16 mol-%) were used in all reactions. * gelation of reaction mixture

#	Tem-perature [°C]	solvent	Reaction time [h]	Monomer conc. [g/mol]	$M_{n,\,SEC}$ [kg/mol]	$M_{w,\,SEC}$ [kg/mol]	$Đ$	Yield [%]
1	100	toluene	72	0.3	14.3	26.0	1.8	93
2	100	toluene	22*	0.5	13.1	23.0	1.8	81
3	100	toluene	72	0.5	11.8	18.5	1.6	79
4	100	mesitylene	6*	0.5	18.1	36.9	2.0	90
5	120	mesitylene	72	0.5	15.6	42.6	2.7	75

Size exclusion chromatography

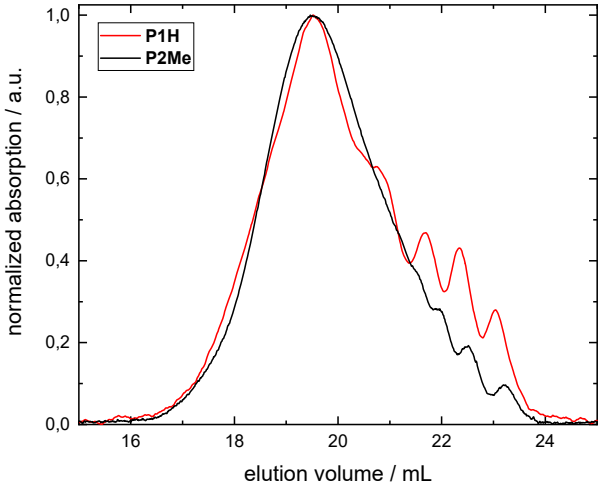

Figure S1. SEC curves ($CHCl_3$, room temperature) of samples PThDPPThF4 (P1H) and PThDPPMeThF4 (P2Me).

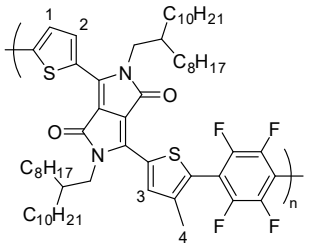

PThDPPMeThF4

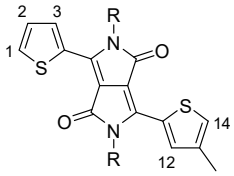

ThDPPMeTh

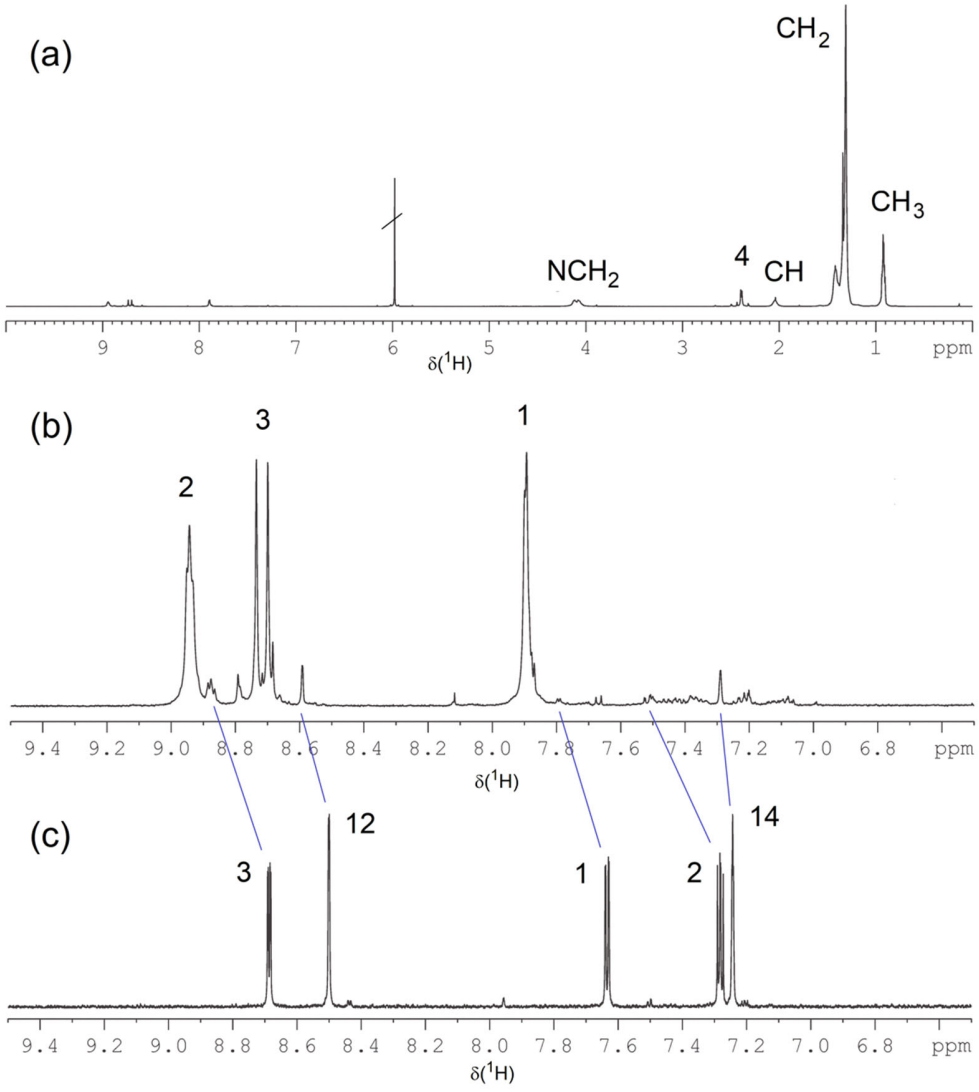

Figure S2. ^{1}H NMR spectrum of PThDPPMeThF4 (P2Me) (a,b) and ThDPPMeTh (region, c) in $C_2D_2Cl_4$ at 120°C. Several signals of PThDPPMeThF4 show a splitting due to the different triads. The lines point to signals of the –DPPTh (1 – 3, less intense) and –DPPMeTh end group (12 and 14, more intense).

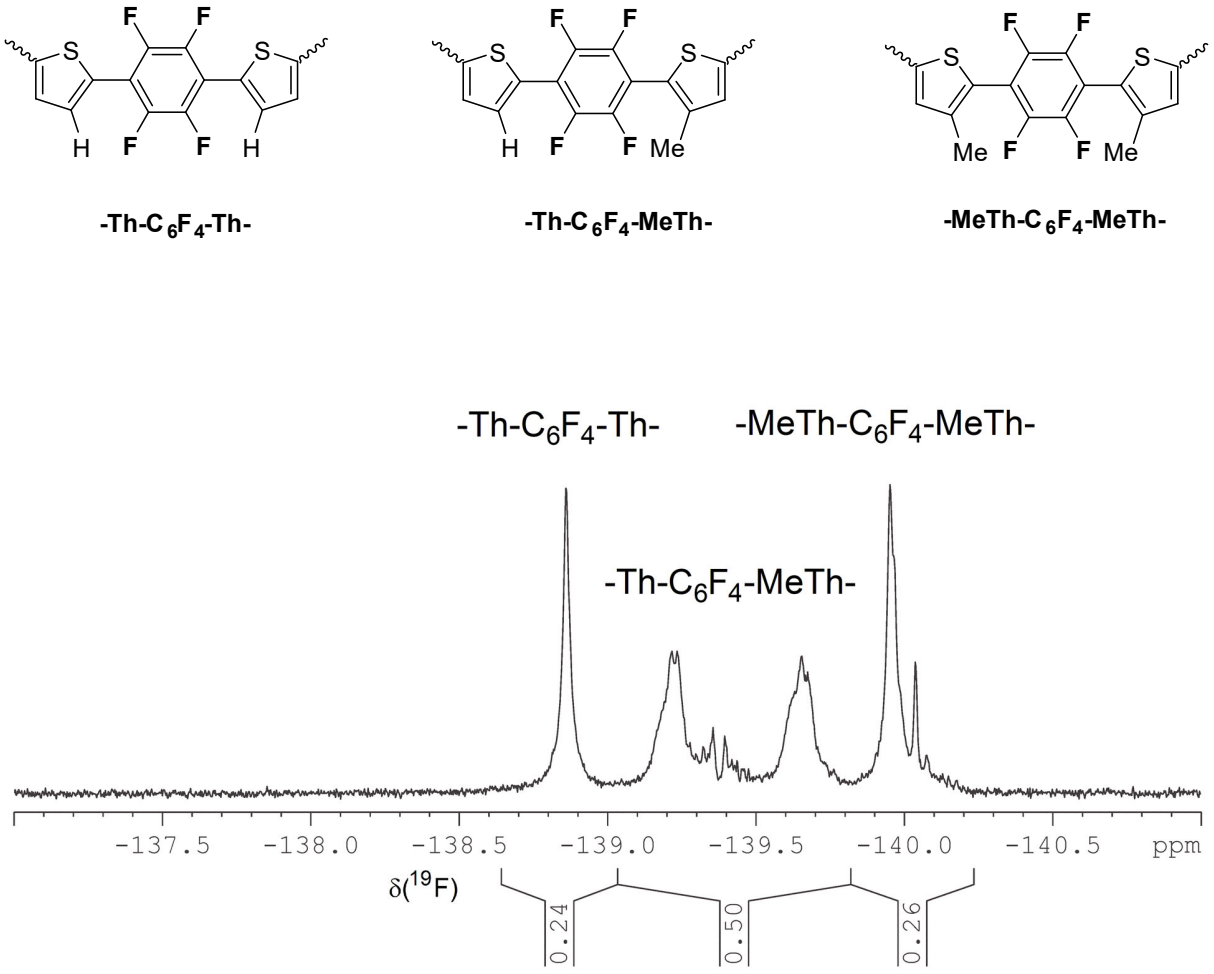

Figure S3. ^{19}F NMR spectrum of PThDPPMeThF4 (P2Me) in $C_2D_2Cl_4$ at 120°C showing the signals of the three C_6F_4-centred triads.

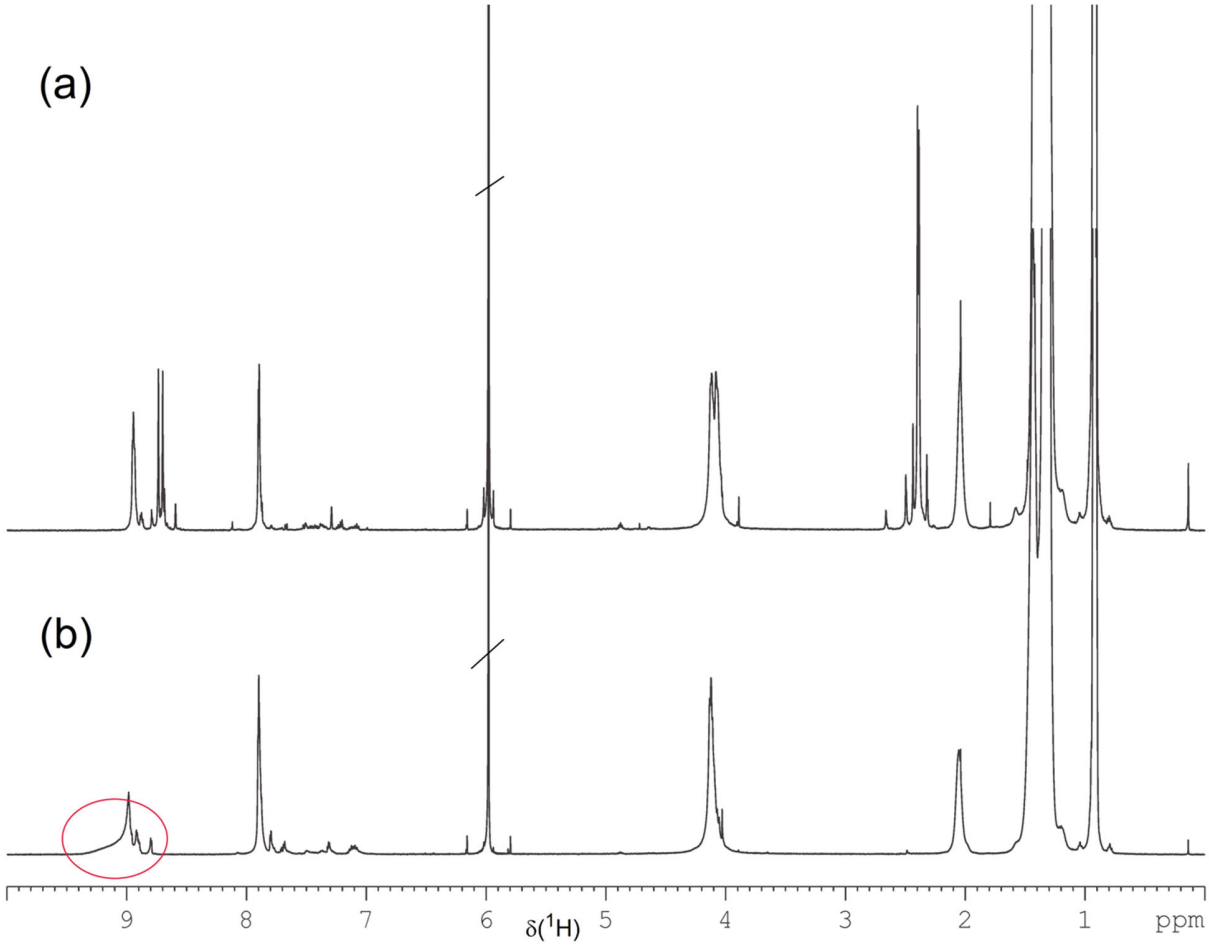

Figure S4. ^{1}H NMR spectrum of PThDPPMeThF4 (P2Me) (a) and PThDPPThF4 (P1H) (b) in $C_2D_2Cl_4$ at 120°C. Note the line broadening observed for the thiophene protons next to the DPP unit of PThDPPThF4 due to association.

Thermogravimetric analysis

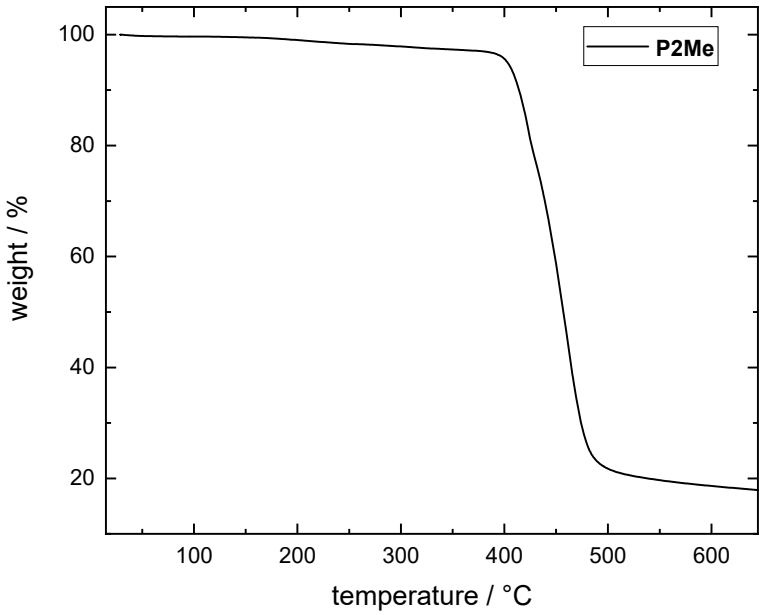

Figure S5. Thermogravimetric analysis (TGA) of PThDPPMeThF4 (P2Me) in N_2 atmosphere and a heating rate of 10 K/min.

Additional UV-Vis spectra

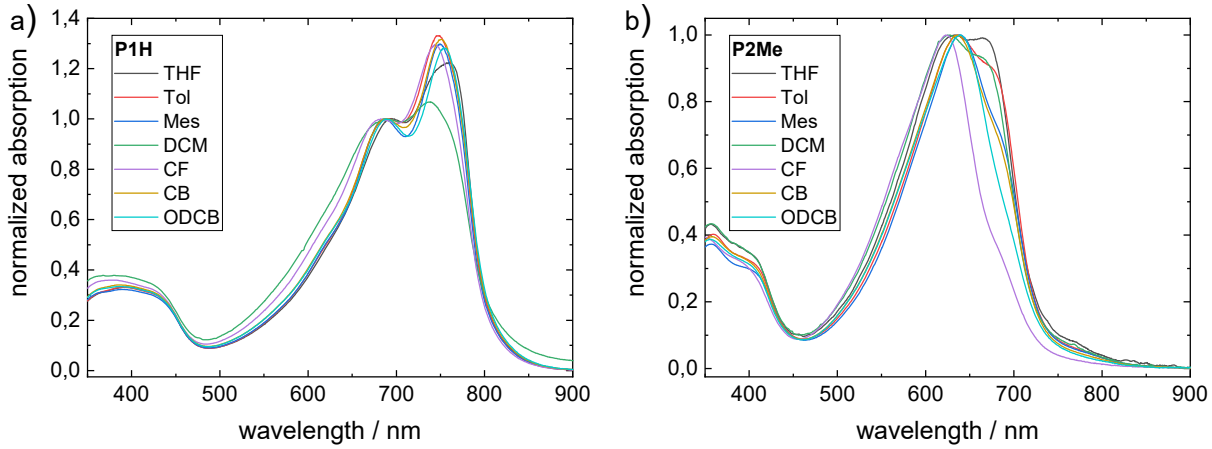

Figure S6. Solvent-dependent UV-Vis spectra of a) PThDPPThF4 (P1H) and b) PThDPPMeThF4 (P2Me) at room temperature (c = 0.02 mg·mL^{-1}).

Additional GIWAXS data

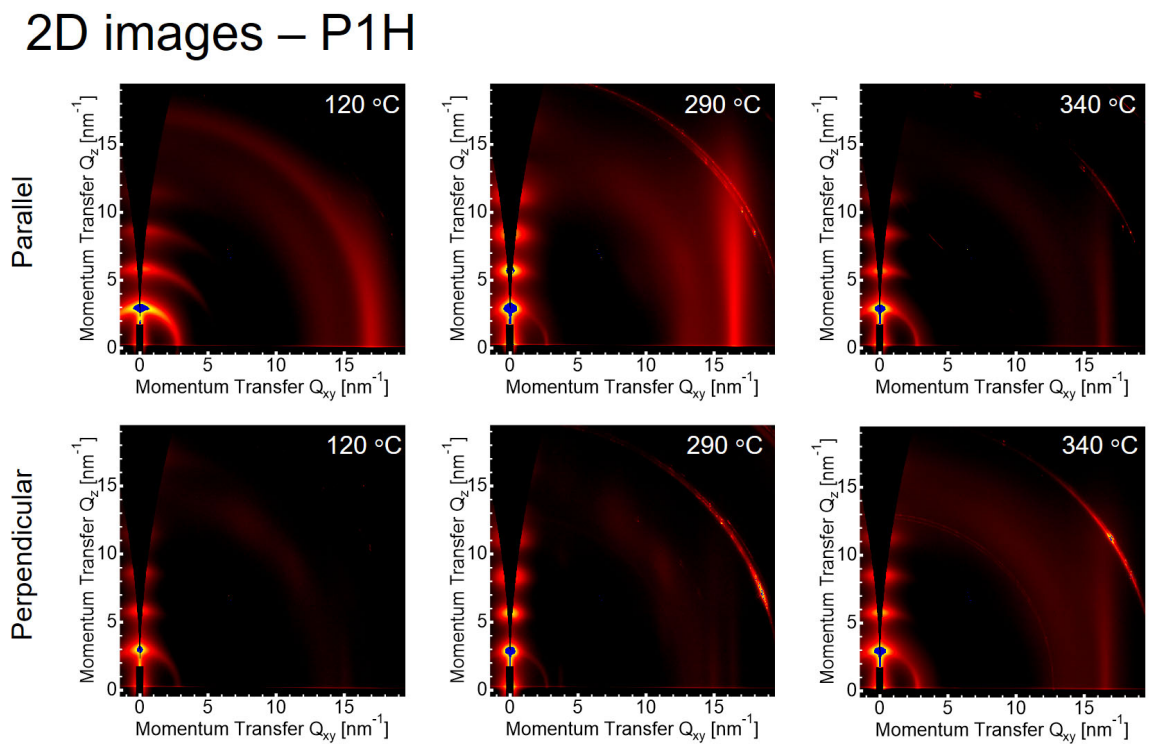

Figure S7. 2D GIWAXS images of P1H annealed at different temperatures.

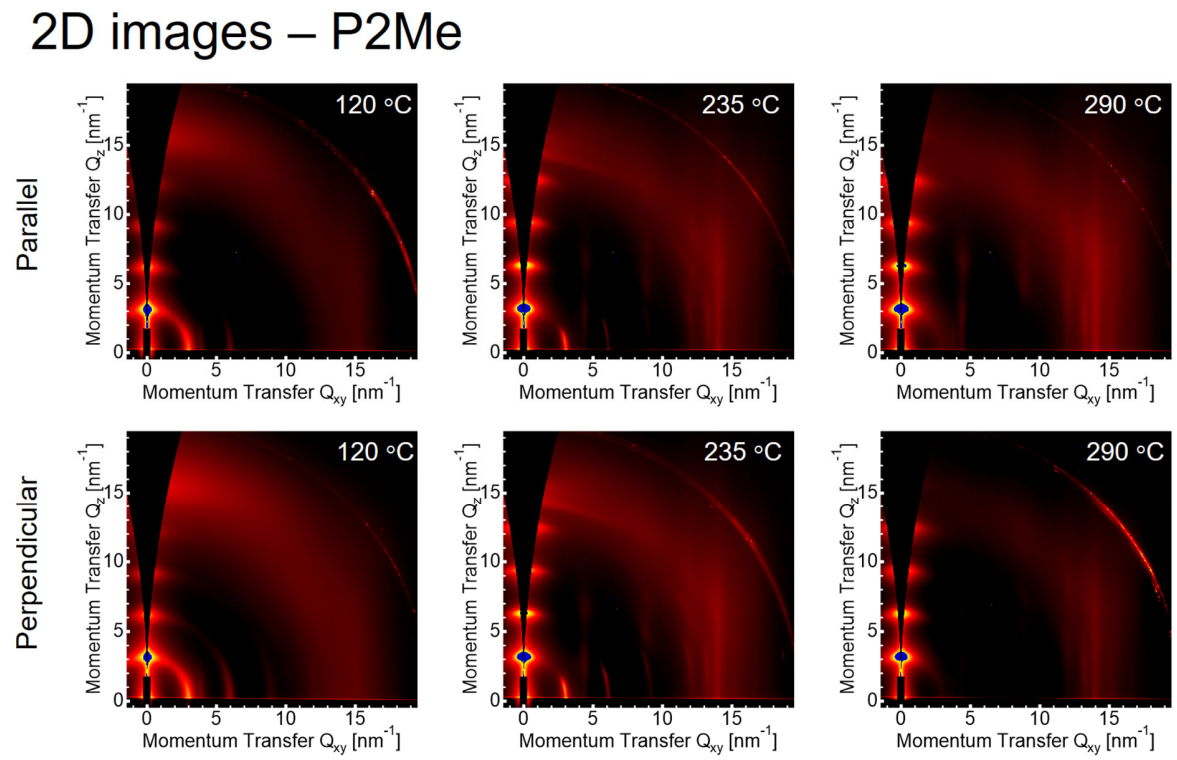

Figure S8. 2D GIWAXS images of P2Me annealed at different temperatures.

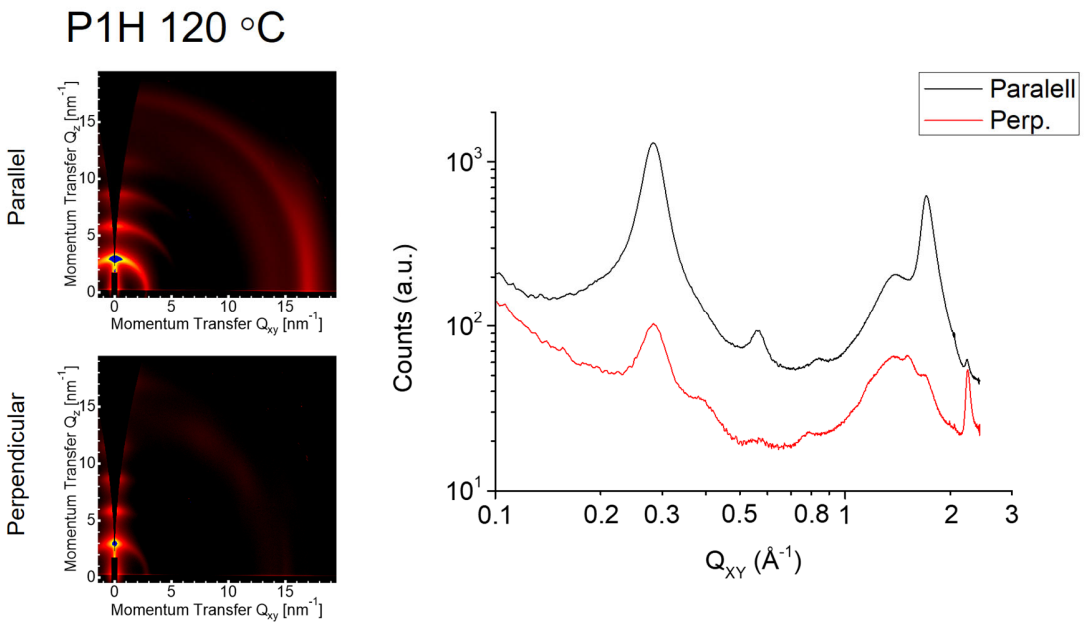

Figure S9. GIWAXS data of P1H annealed at 120 °C.

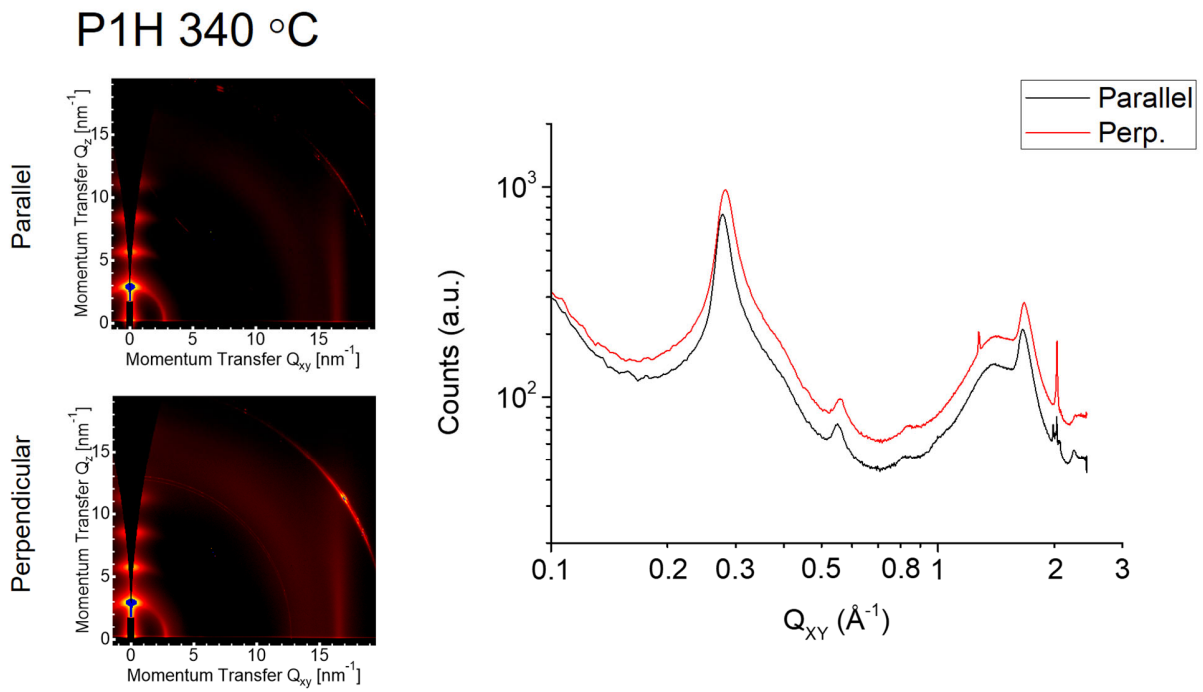

Figure S10. GIWAXS data of P1H annealed at 340 °C.

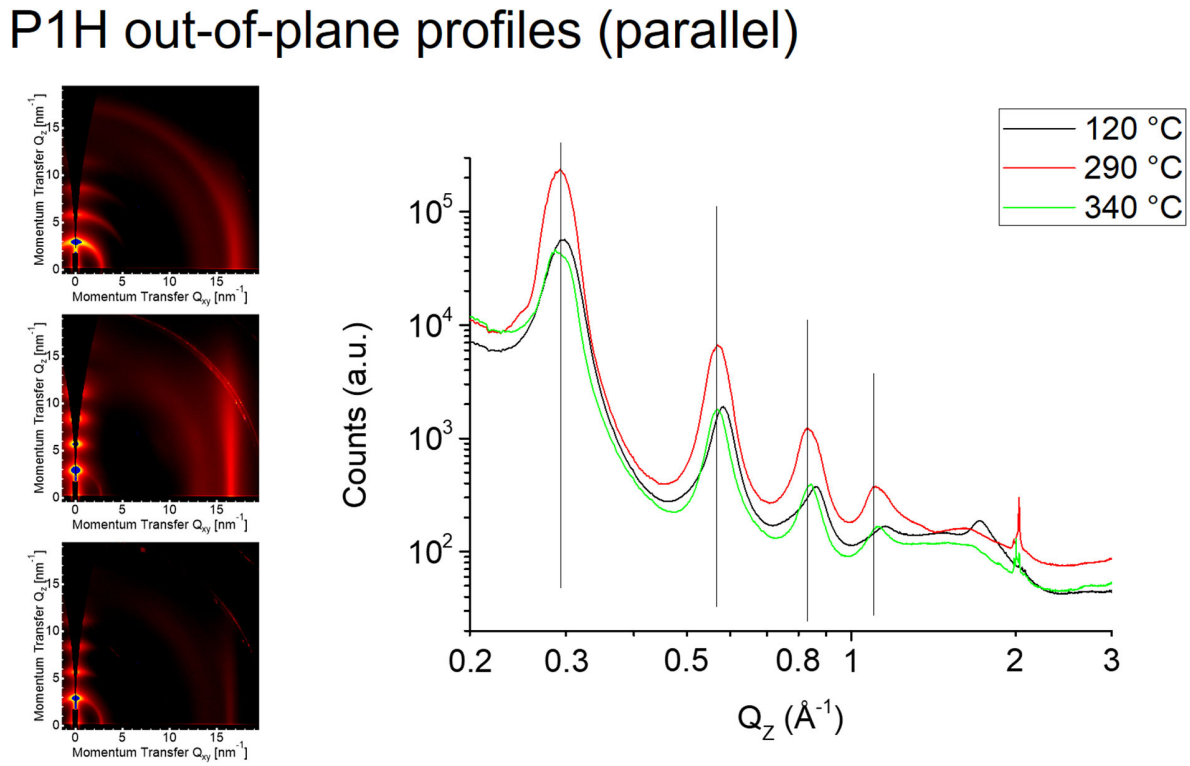

Figure S11. Comparison of out-of-plane profiles for P1H annealed at different temperatures.

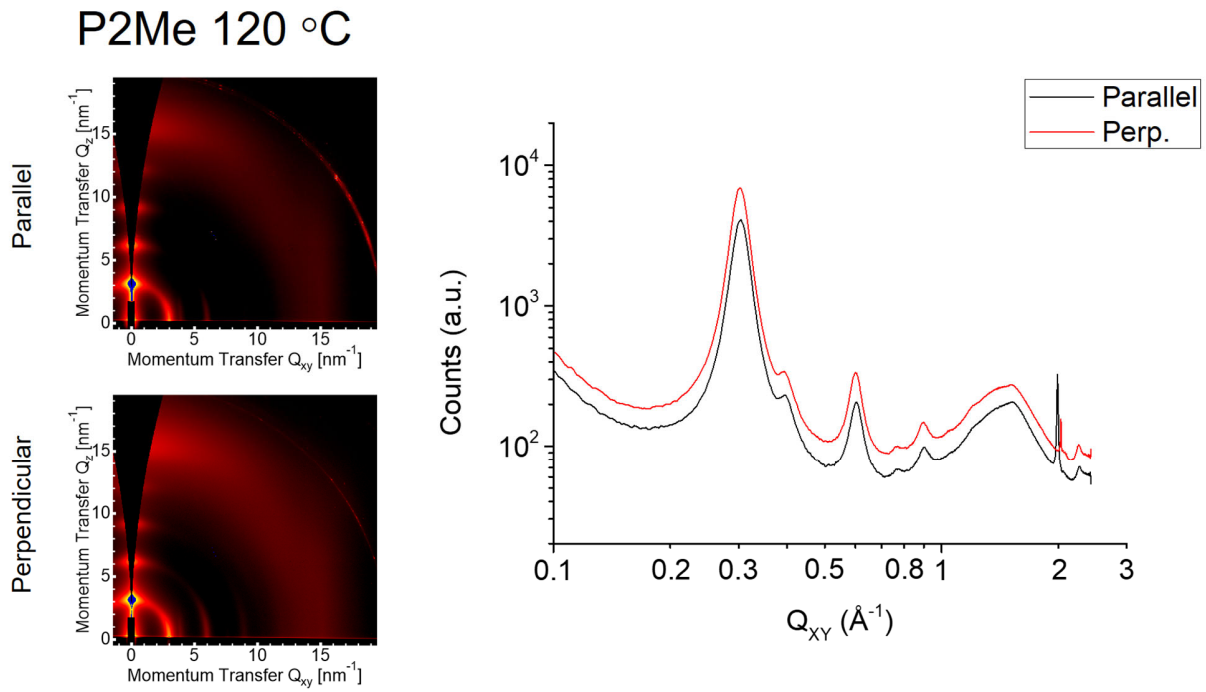

Figure S12. GIWAXS data of P2Me annealed at 120 °C.

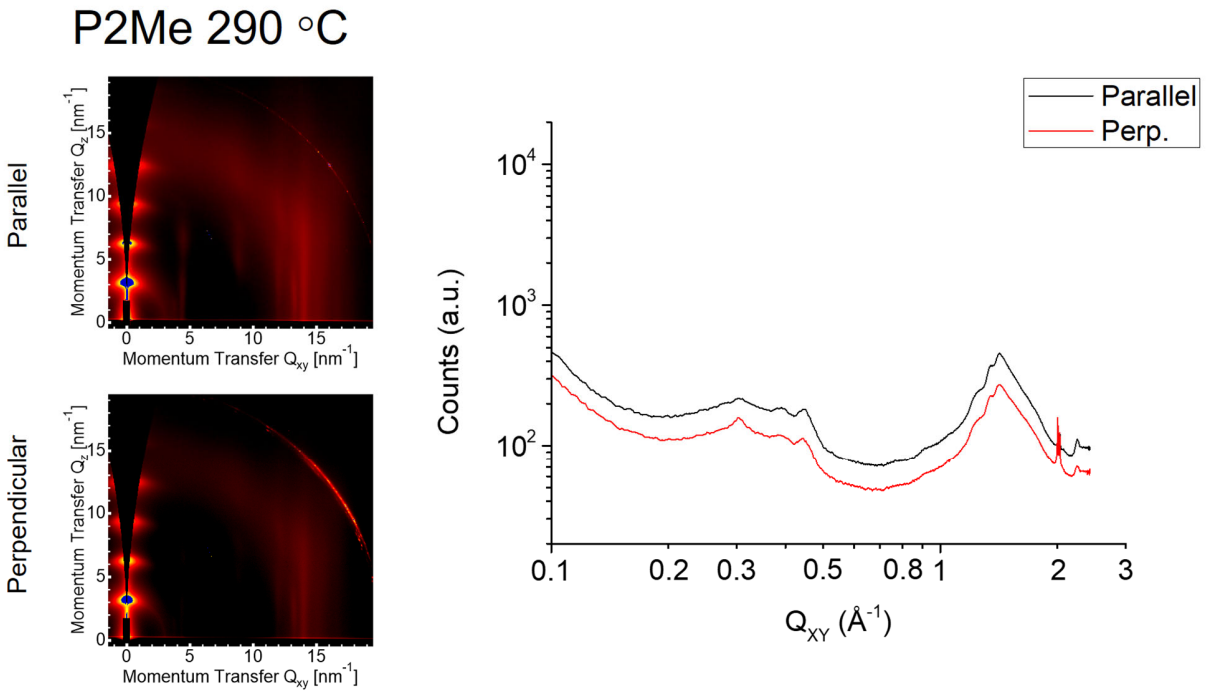

Figure S13. GIWAXS data of P2Me annealed at 290 °C.

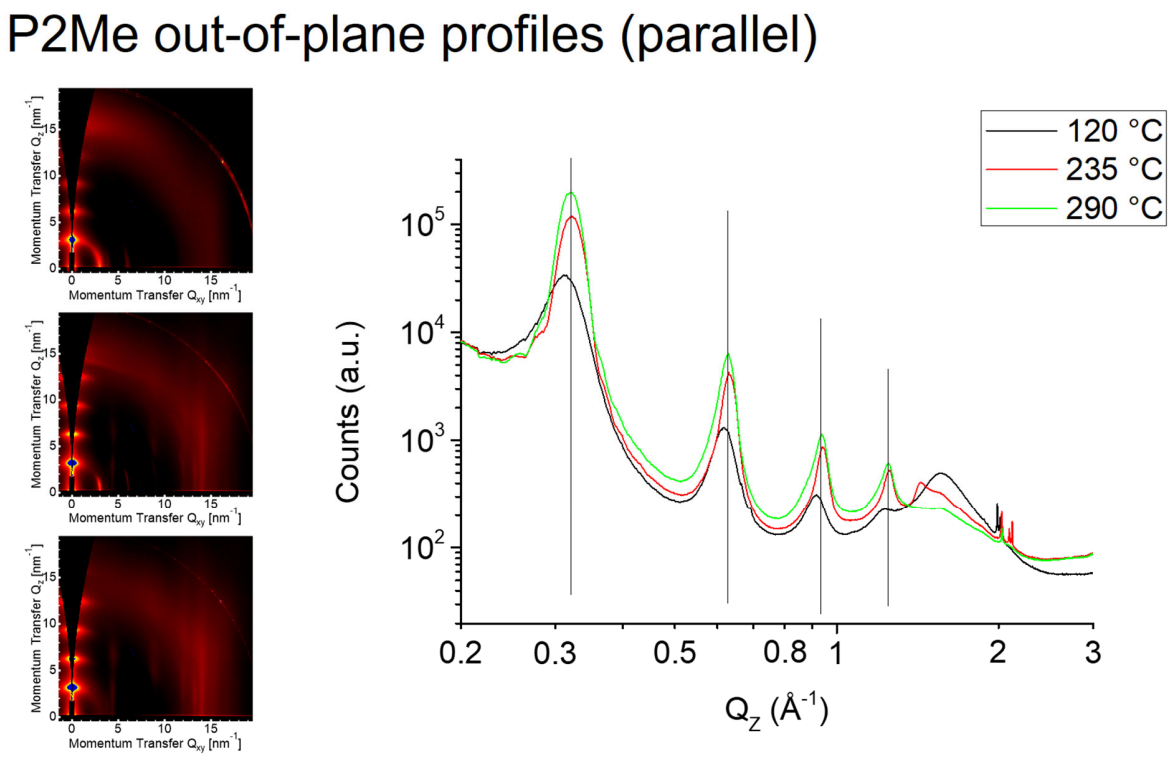

Figure S14. Comparison of out-of-plane profiles for P2Me annealed at different temperatures.

C) ^{1}H and ^{13}C NMR Spectra

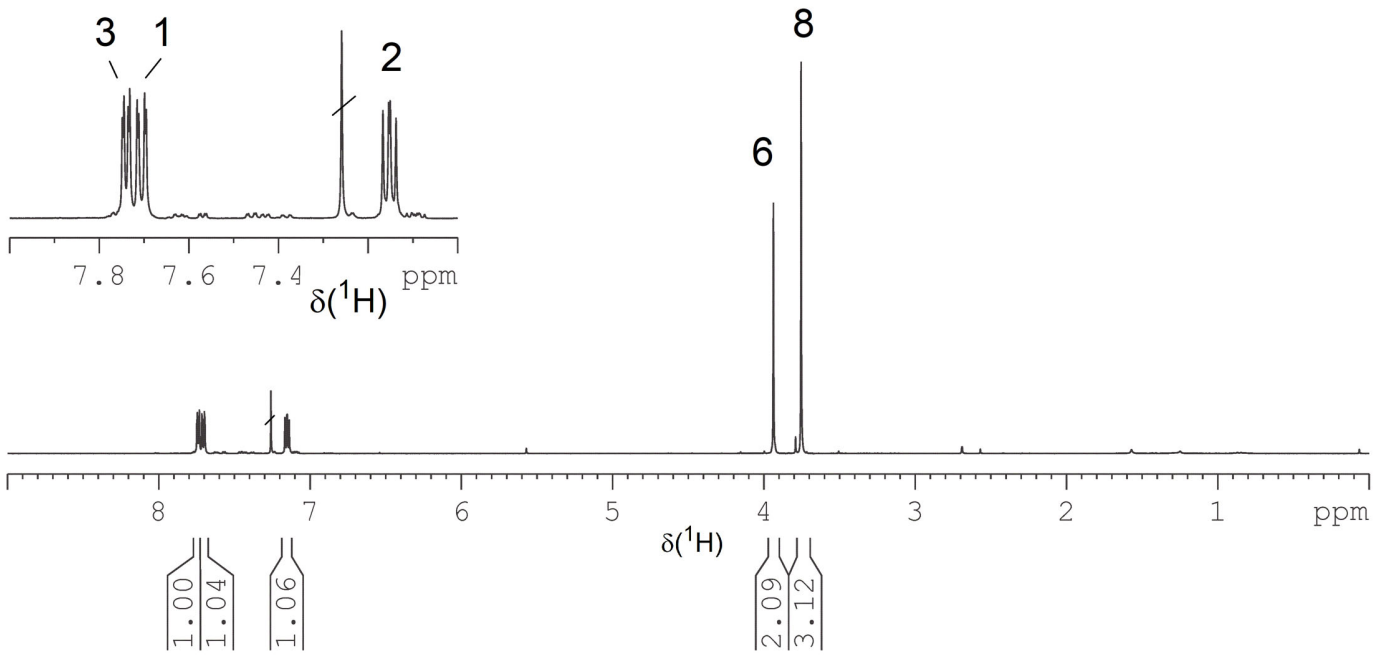

Figure S15. ^{1}H NMR spectrum of **1** in $CDCl_3$.

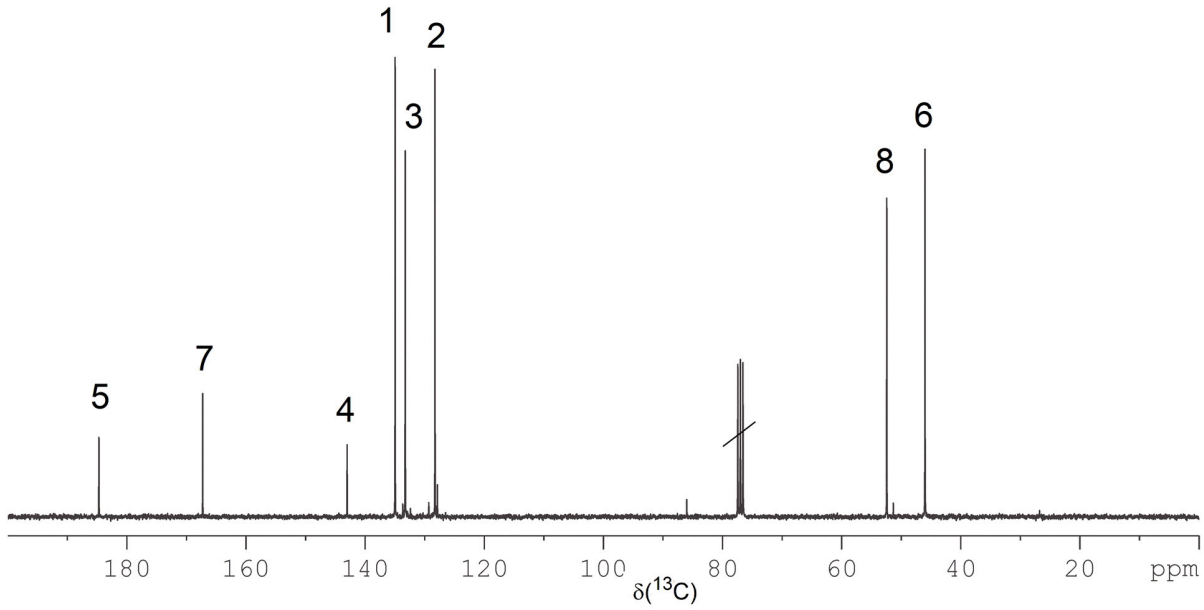

Figure S16. ^{13}C NMR spectrum of **1** in $CDCl_3$.

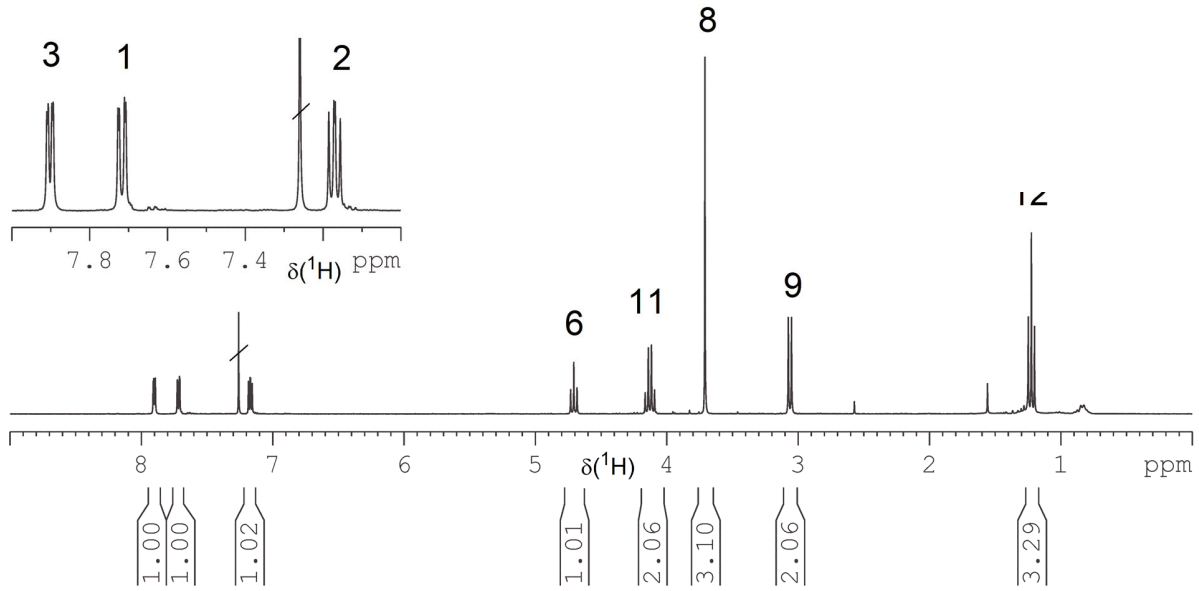

Figure S17. ^{1}H NMR spectrum of **2** in $CDCl_3$

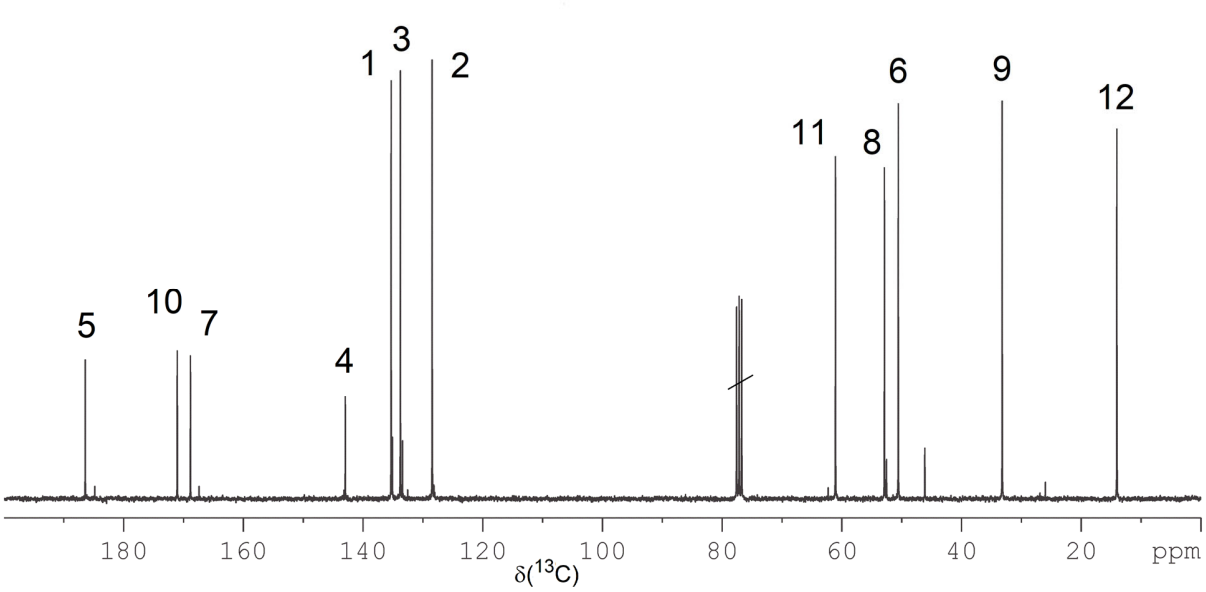

Figure S18. ^{13}C NMR spectrum of **2** in $CDCl_3$.

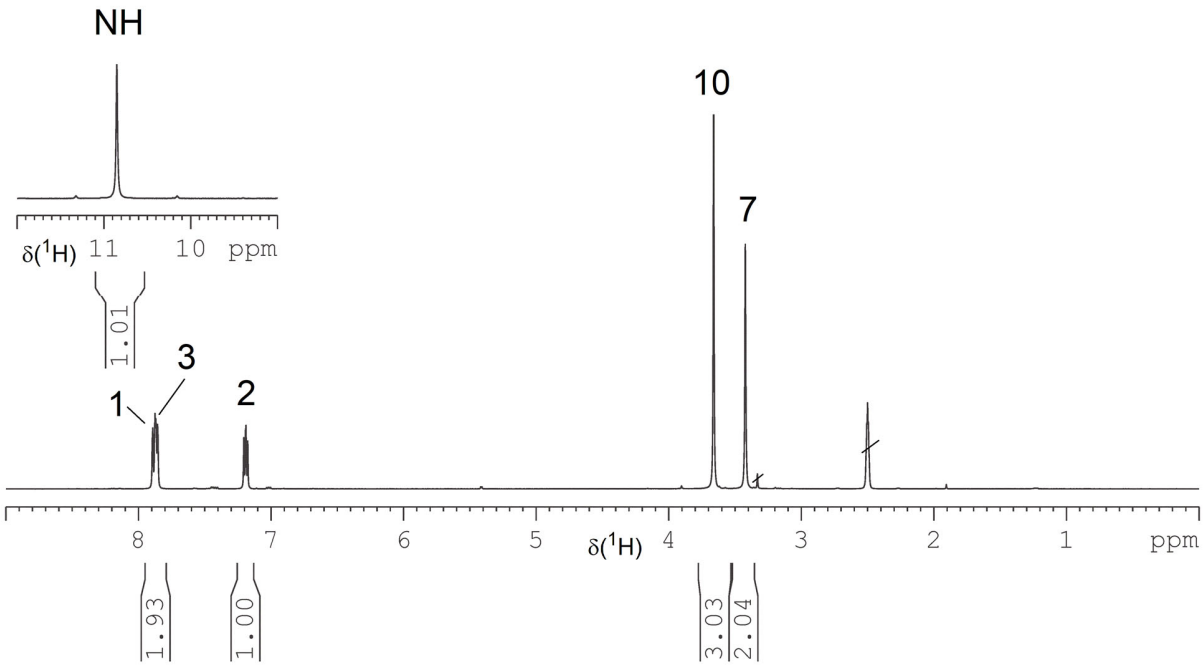

Figure S19. ^{1}H NMR spectrum of **3** in DMSO-d$_6$.

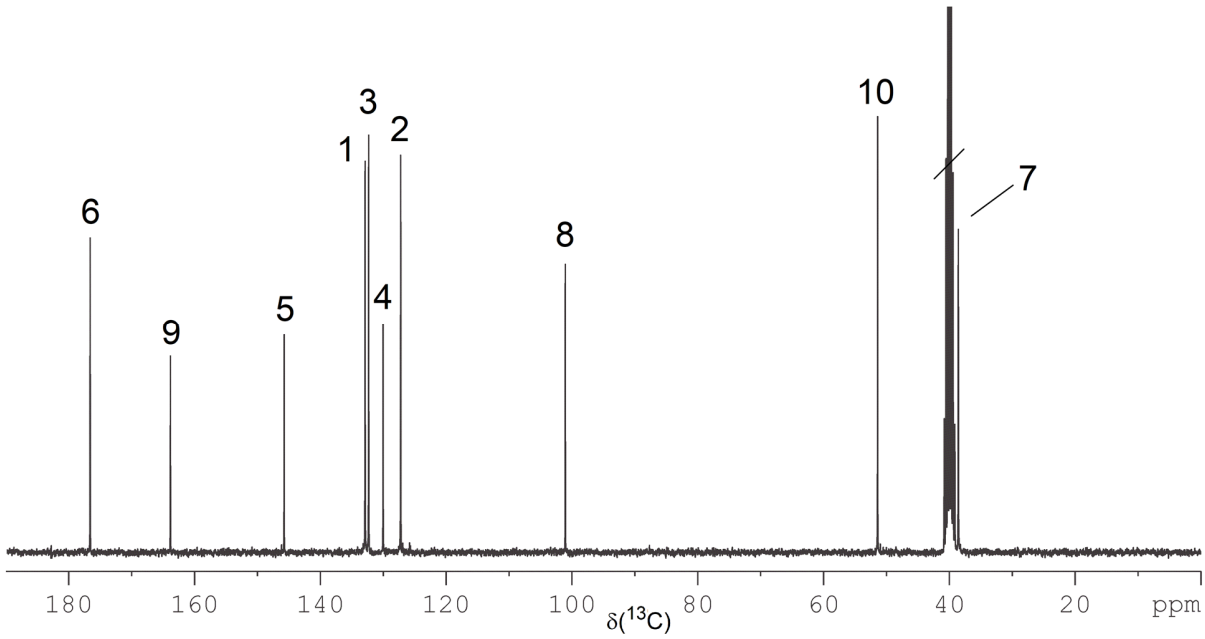

Figure S20. ^{13}C NMR spectrum of **3** in DMSO-d$_6$.

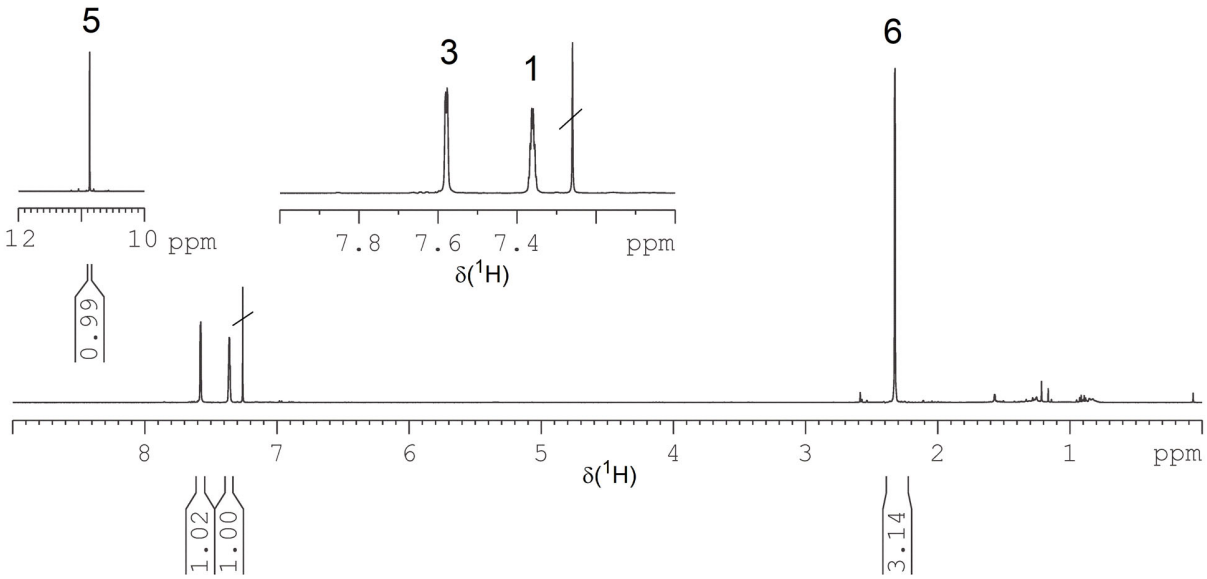

Figure S21. ^{1}H NMR spectrum of **4** in $CDCl_3$.

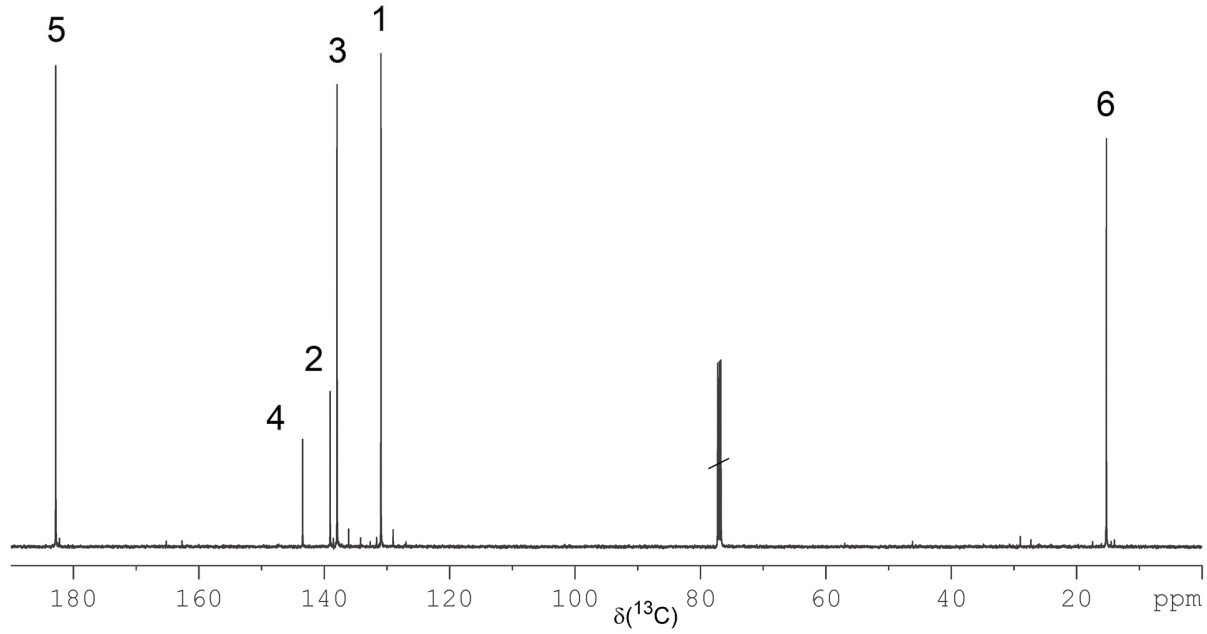

Figure S22. ^{13}C NMR spectrum of **4** in $CDCl_3$.

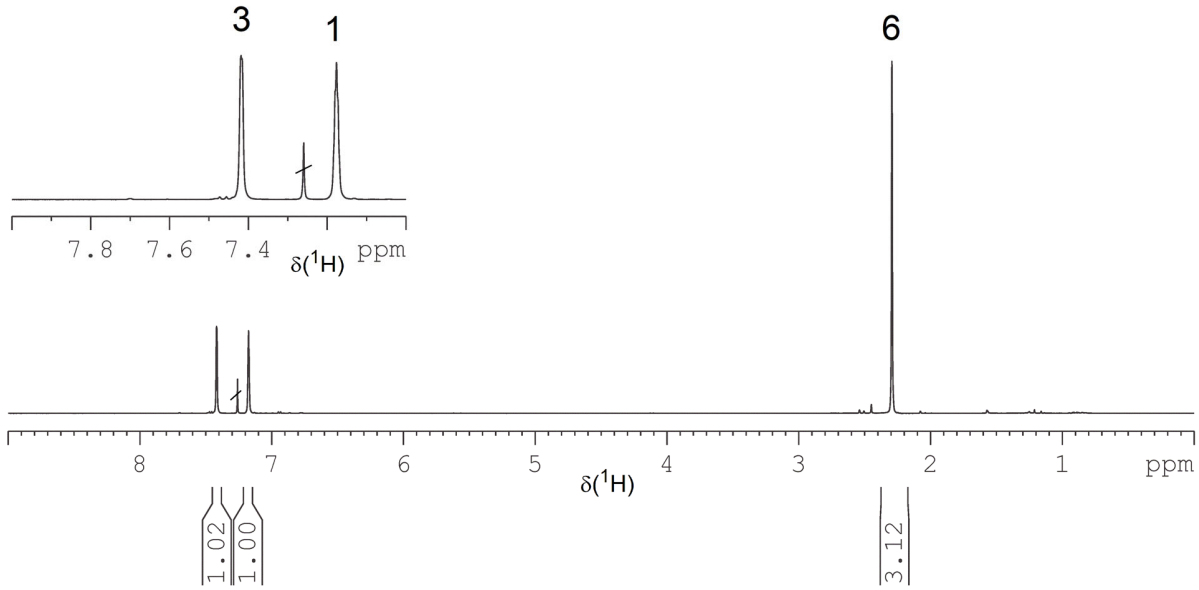

Figure S23. ^{1}H NMR spectrum of **5** in $CDCl_3$.

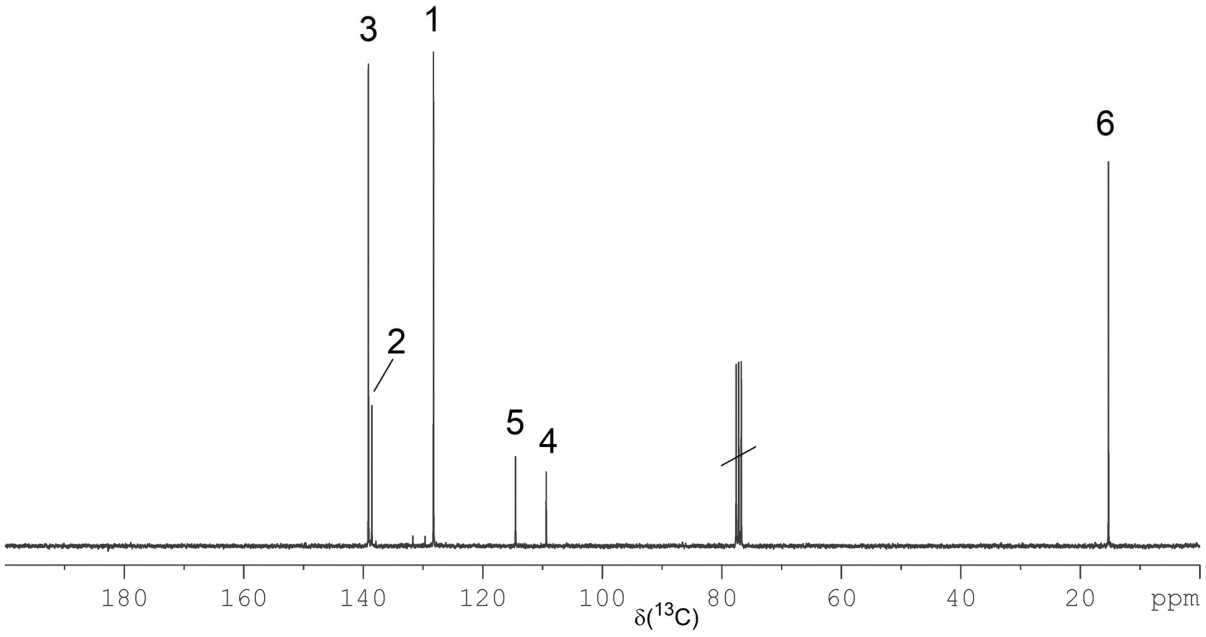

Figure S24. ^{13}C NMR spectrum of **5** in $CDCl_3$.

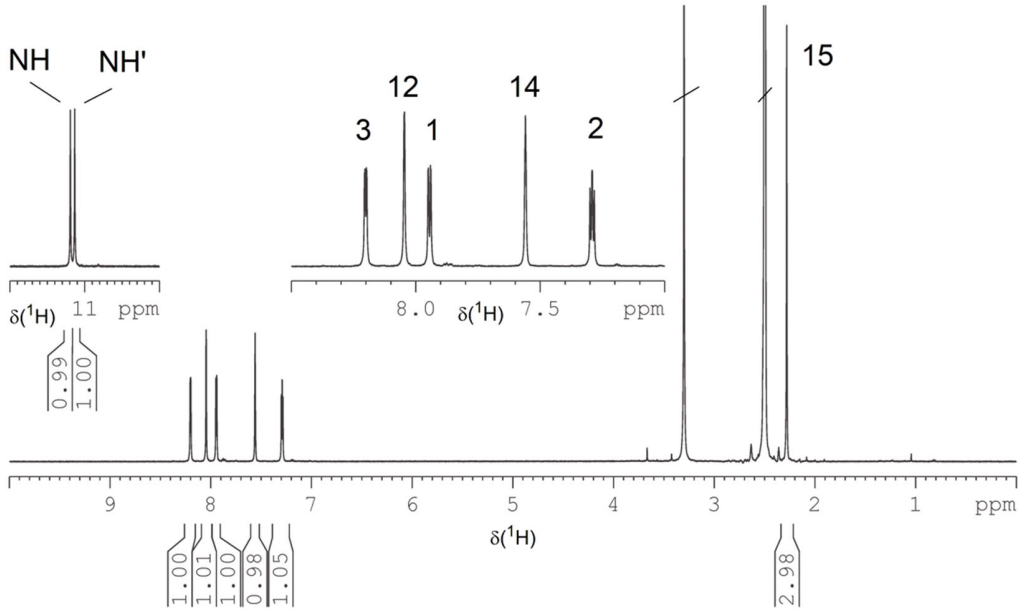

Figure S25. ^{1}H NMR spectrum of **6** in DMSO-d$_6$.

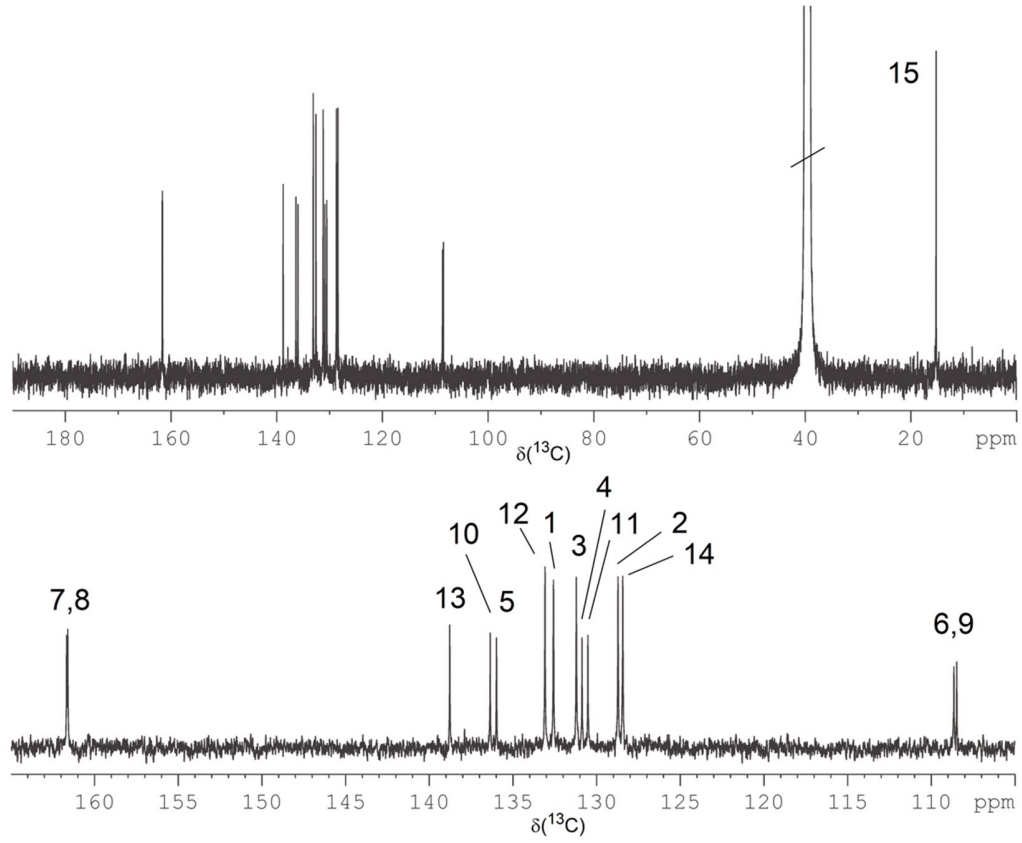

Figure S26. ^{13}C NMR spectrum of **6** in DMSO-d$_6$.

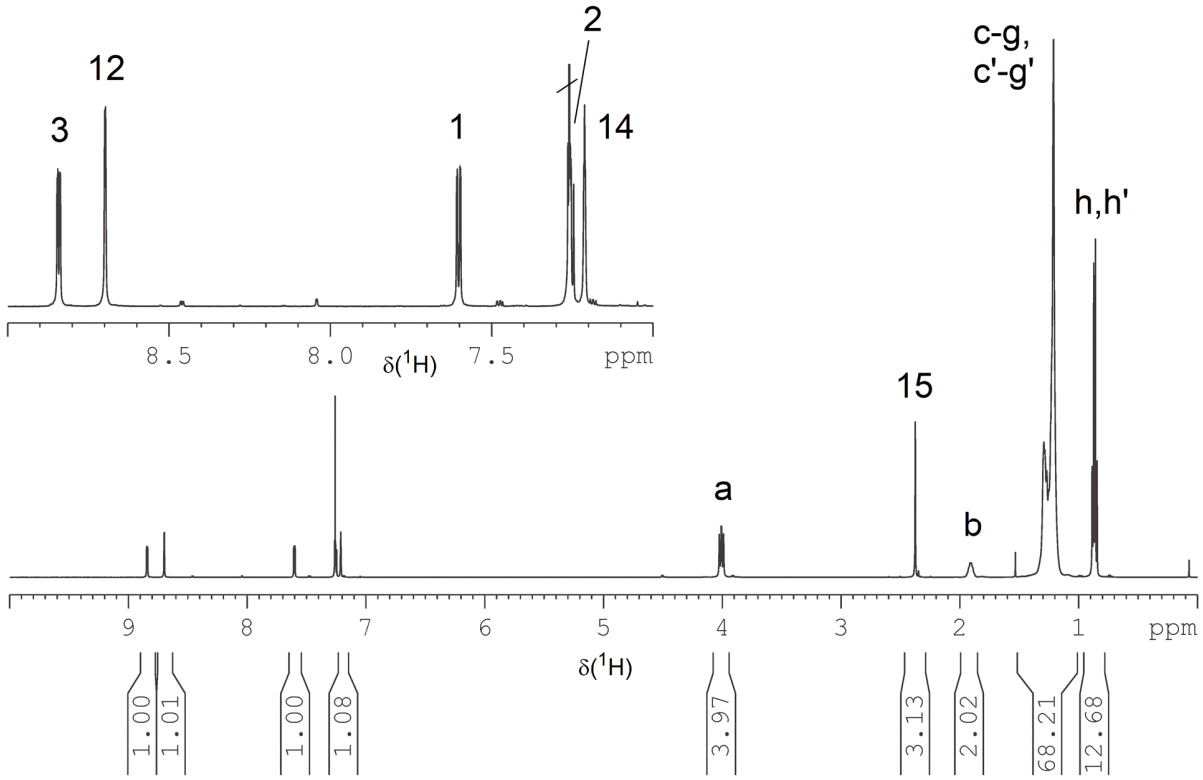

Figure S27. ^{1}H NMR spectrum of ThDPPMeTh in $CDCl_3$.

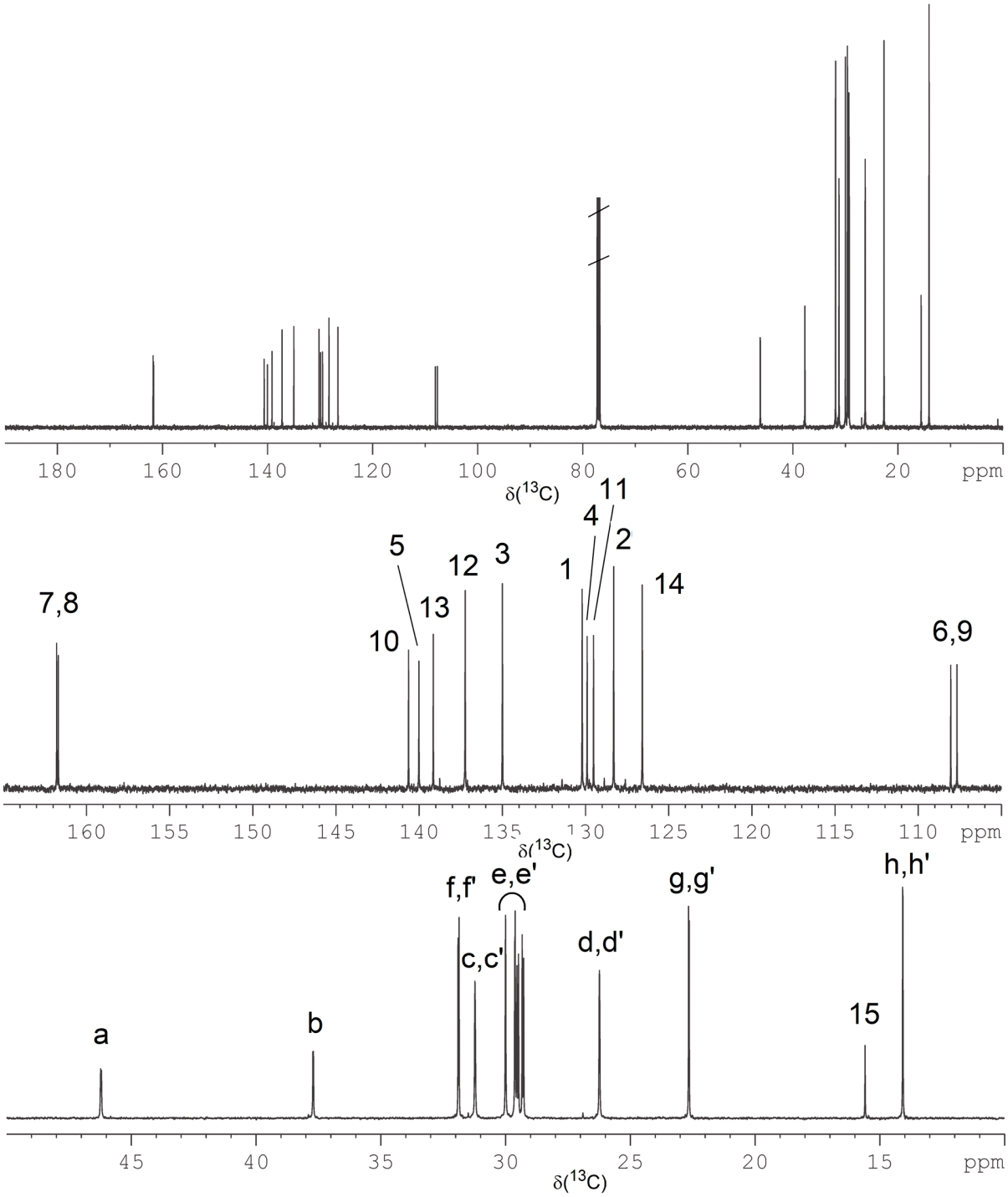

Figure S28. ^{13}C NMR spectrum of ThDPPMeTh in $CDCl_3$.

D) Supporting References

[1] C. Bannwarth, E. Caldeweyher, S. Ehlert, A. Hansen, P. Pracht, J. Seibert, S. Spicher, S. Grimme, *WIREs Comput. Mol. Sci.* **2021**, *11*, e1493.

[2] F. Neese, *WIREs Comput. Mol. Sci.* **2022**, *12*, e1606.

[3] N. M. Kirby, S. T. Mudie, A. M. Hawley, D. J. Cookson, H. D. T. Mertens, N. Cowieson, V. Samardzic-Boban, *J. Appl. Crystallogr.* **2013**, *46*, 1670.

[4] J. Ilavsky, *J. Appl. Crystallogr.* **2012**, *45*, 324.